RSC Advances

ROYAL SOCIETY OF CHEMISTRY

www.rsc.org/advances

Catalytic oxidation of acetone over $CuCeO_x$ nanofibers prepared by electrospinning method

Rui Qin, Jinghuan Chen, Xiang Gao *, Xinbo Zhu, Xinning Yu, Kefa Cen
State Key Laboratory of Clean Energy Utilization of Zhejiang University, Hangzhou, 310027, P.R. China

Abstract

A series of $CuCeO_x$ nanofibers catalysts with different Cu/(Cu+Ce) molar ratios were synthesized by electrospinning method. The catalysts were evaluated for acetone oxidation at different temperatures (100-280 ℃) with a GHSV of 79,000 ml/(g ħ). The results showed that nanofibers catalysts possessed better catalytic performance than catalysts prepared by urea-nitrate combustion and sol-gel methods. Appropriate Cu/(Cu+Ce) molar ratio could greatly improve the activity of nanofibers catalyst, and a significant improvement of the activity was obtained on $Cu_{0.50}Ce_{0.50}O_x$ nanofibers catalyst (~100% acetone conversion at 270 ℃). Characteristic analysis suggested (1) special nanofibrous morphology with large specific surface area; (2) abundant oxygen vacancies and (3) cerium ions with unusual oxidation states were the main factors that would affect catalytic activity of $CuCeO_x$ nanofibers catalysts.

Keywords: acetone; catalytic oxidation; $CuCeO_x$; nanofibers; electrospinning

1 Introduction

Volatile organic compounds (VOCs) are massively emitted via human activities like industry production, fuel combustion and oil storage. VOCs are precursors of photochemical smog which threat environment and human health seriously. Exposure to VOCs may cause carcinogenic, mutagenic, and teratogenetic effects on human body due to their toxicity[1]. Researchers have explored various methods for VOCs elimination[2-4], among these strategies, catalytic oxidation is one of the most effective and economic ways for VOCs abatement in large volumes of air[5]. In this study, acetone was selected as the model VOC since it's one of the most abundant VOC in the atmosphere[6].

Noble metals and transition metal oxides have been studied for VOCs catalytic oxidation extensively in recent decades[7]. Noble metals have been proven to be more active at low temperatures than transition metal oxides, but their high cost and low resistance to halogens limit their application[8, 9]. Otherwise, some transition metal oxide catalysts have also been found to be active for VOCs catalytic oxidation[10, 11]. Among them, copper oxide and cerium oxide catalysts were researched intensively. Since copper oxide catalysts possess high activity for VOCs catalytic oxidation[12] and cerium oxide catalysts have high oxygen storage capacity and facile reducibility of Ce^{4+}/Ce^{3+} compared to other fluorite-type oxides[13]. In addition, researchers even found that Cu-Ce binary metal oxide catalysts possess high activity which is even comparable to supported noble metal catalysts for oxidation reactions, as the shift between Ce^{4+} and Ce^{3+} becomes easier when transition metal ions are added in ceria lattice[14-16].

Various methods have been used in preparation of metal oxide catalysts, including sol-gel, combustion methods and so on. However, these catalysts have relatively low specific surface area and their microstructure inhibits the diffusion, adsorption and desorption process of molecules to some extent. As is known, nanofibers catalysts are widely used in photocatalytic reactions since they possess large specific surface area and one-dimensional nanofibrous morphology which can promote the mass transfer process during reactions[17, 18]. Therefore, in order to improve catalytic performance, it is necessary to find an appropriate method to synthesize metal oxide nanofibers catalysts. Among variety of techniques,

electrospinning technique has been proven an effective way to produce fibrous metal oxide in nanoscale[19, 20]. This processing involved the following steps：(1) preparation of sol solution with a suitable inorganic precursor and polymer content, and achieving the right rheology for electrospinning; (2) spinning of the solution to obtain polymer/inorganic fibers; and (3) calcinations of the composite fibers to obtain final oxide nanofibers [20].

In this work, one-dimensional $CuCeO_x$ nanoscale fibers with different Cu/(Cu+Ce) ratios were successfully prepared by electrospinning method. The morphological, structural and chemical characteristics of the catalysts were investigated by SEM, EDX, TEM, XRD, XPS, N_2 sorption, H_2-TPR, and the catalytic performance for acetone oxidation was examined in a fixed-bed reactor. The results showed that electrospinning method endowed $CuCeO_x$ nanofibers catalysts with specific one-dimensional nanofibrous morphology. Then the relationship between structure and catalytic performance for acetone oxidation was tried to establish. In addition, this study may be helpful for designing or synthesizing novel metal oxide catalysts and expand the application of metal oxide catalysts in filtration and separation[21].

2. Experimental

2.1 Catalyst preparation

$CuCeO_x$ nanofibers catalysts were synthesized via electrospinning method. Firstly, appropriate amount of $Ce(NO_3)_3$ $6H_2O$ and $Cu(NO_3)_2$ $3H_2O$ was dissolved in 6ml anhydrous alcohol and 10 ml deionized water simultaneously. Total nitrate salts were 0.01 mol and the molar ratios of Cu/(Cu+Ce) were 0, 0.15, 0.30, 0.50, 0.70 and 0.85. (It should be mentioned that because for the same preparation process, the viscosity of sol solution of pure $Cu(NO_3)_2$ $3H_2O$ is too low to adapt to our electrospinning process. Thus the preparation of pure CuO nanofibers is not available.) After magnetically stirring for 1 h, 2 g Polyvinylpyrrolidone (PVP, Mw=1,300,000) was added in the solution. Then the mixtures were agitatedly stirred for 12 h at room temperature to obtain a homogenous and translucent solution. CuCe/PVP as-spun nanofibers were prepared by electrospinning the viscous sol-gel solution between a syringe and an aluminum foil attached on a roller (rotating speed 100 rpm). The distance between the tip of spinneret (21G) and the aluminum foil was 150 mm. A DC high-voltage supply connected on the needle generated negative voltage of 15 kV and

the flow rate was controlled by a syringe pump at constant 0.5 ml/h. This electrospinning process was carried out in air ambient at room temperature. Then the as-spun fibers were dried at 20 ℃ for 24 h and calcined in air at 500 ℃ for 4 h to obtain $CuCeO_x$ nanofibers (denoted as NFs).

For comparison, the $CuCeO_x$ catalysts with Cu/(Cu+Ce) molar ratio of 0.5 were also prepared by urea-nitrate combustion (denoted as cmb) and sol-gel (denoted as sol) methods[13, 22].

2.2 Catalyst characterizations

Field emission scanning electron microscopy (FE-SEM) images and Energy dispersive X-ray spectroscopy (EDX) data were recorded on a SIRION microscope with a voltage of 25 kV coupled to an X-ray detector.

Transmission electron microscopy (TEM) was performed using a Hitachi H-9500 microscope operating with an acceleration voltage of 300 kV. For the TEM measurement, the samples were prepared by ultrasonication in ethanol, evaporating a drop of the resultant suspension onto a carbon-coated copper grid.

BET surface areas were measured by N_2 adsorption and desorption at liquid nitrogen temperature (77 K) with Autosorb-1-C (Quantachrome Instrument Crop.). All samples were degassed under vacuum at 300 ℃ for 2h before the measurement.

X-ray diffraction (XRD) patterns were recorded on a PANalytical X'Pert PRO XRD system using Cu Kα radiation (λ= 0.15418 nm) in the 2θ range of 10–80° (scanning rate of 4 °/min).

X-ray photoelectron spectroscopy (XPS) data were obtained with a Thermo ESCALAB 250Xi using Al Kα as the exciting radiation at constant pass energy of 1486.6 eV. The binding energies were calculated with reference to the energy of C 1s peak of contaminant carbon at 284.6 eV.

Temperature programmed reduction of hydrogen (H_2-TPR) experiments were performed in quartz reactor in 10% H_2/Ar with a flow rate of 30ml/min, and 15mg of catalyst was used. Prior to reduction, catalyst was heated in a 10% O_2/Ar flow (30 ml/min) from room temperature to 300 ℃ and held for 30 min, and then treated in Ar stream at room temperature for 30 min to remove any residual oxygen. The samples were heated from 50 ℃ to 850 ℃ at a flow rate of 10 ℃/min. The amount of H_2 consumption was measured using a thermal conductivity detector (TCD).

2.3 Catalytic activity

All catalytic performance tests were performed in a fixed bed tubular quartz reactor (6 mm i.d.) at atmospheric pressure. 35 mg of the catalyst (40-60 mesh) was placed in the middle of the reactor and total flow rate was kept at 46ml/min, corresponding gas hourly space velocity (GHSV) was 79,000 ml/(g h). The feed gas mixture contained 500 ppm acetone, 5% O_2, and balanced N_2. The temperatures of the catalyst bed and tubular electric furnace were monitored automatically by E-type thermocouples. The inlet and outlet concentration of acetone were analyzed on-line by a gas chromatograph (Agilent 7890A, USA) equipped with a flame ionization detector (FID) and a capillary column of HP-Innowax (Agilent, USA) operated at 60 ℃. The acetone removal efficiency ($\eta_{acetone}$) is calculated as follows:

$$\eta_{acetone}(\%) = \frac{c_{in} - c_{out}}{c_{in}} \times 100\%$$

c_{in}, c_{out} —inlet and outlet concentration of acetone

Blank test was conducted with crushed quartz sand (40-60 mesh) to guarantee the credibility of this test. The results showed no thermal destruction of acetone was detected in the same feed gas below 280 ℃. Before each test, catalysts were firstly put in the fixed-bed tube with the feed stream passing and stabilized for 1 h. Then the temperature was increased at a heating rate of 5 ℃/min, and all the data obtained at each temperature were the average of three measurements which were stabilized for 20 min respectively.

3 Results and discussion

3.1 Morphology characterization

The morphology and microstructure of the as-spun (Fig. 1.a-f) and calcinated nanofibers (Fig. 1.A-F) were investigated by SEM. The micrographs demonstrated that the length of nanofibers is on the order of several millimeters, and their average diameters (denoted as D) is on the order of about hundreds of nanometers (Table 1). The pure CeO_2 nanofibers possess one-dimensional nanofibrous morphology and the average diameter of as-spun CeO_2 nanofibers is 610 nm. When copper nitrates were added, the average diameter of as-spun nanofibers decreases. With the increase of Cu/(Cu+Ce) molar ratio from 0.15 to 0.70, the average diameter decreases from 590 to 525 nm. However, when the copper content further increased, several coarse grains are formed on the nanofibers and a part of fibers tangle with each other to form

arachnoid morphology. After calcination, the diameter of nanofibers reduces about 200 nm, probably caused by the decomposition of PVP and formation of copper and cerium oxide crystals during programmed temperature process. With the increase of Cu/(Cu+Ce) molar ratio from 0 to 0.50, the average diameter of calcinated nanofibers decreases from 460 to 295 nm. With further increase of Cu/(Cu+Ce) molar ratio up to 0.70, their fibrous morphology was deformed to arachnoid morphology with coarse grains. When Cu/(Cu+Ce) molar ratio increased up to 0.85, nanofibers lose their nanofibrous morphology completely and form a sheet with coarse surface. The same phenomenon was also found in electrospinning of CuO/TiO_2 nanofibers. Researchers found adding copper salts in sol-gel solution had a negative impact on the nanofibrous morphology[23].

The micro-morphology of nanofibers was further investigated by TEM. As a representative, TEM images of $Cu_{0.50}$-NFs were shown in Fig. 2. Fig. 2.A showed the diameter of the single nanofiber is about 120 nm and the length is more than 1 μm. Additionally, the inner-planar spacing was measured and shown in high resolution TEM (HRTEM) image (Fig. 2.B). The lattice fringes are 0.31 nm, 0.27 nm and 0.23 nm, which correspond well with fringe spacing of CeO_2 (111), (200) (JCPDS 34-0394) and CuO (111) (JCPDS 45-0937) respectively, indicating the presence of CeO_2, CuO nanocystals in the nanofibers.

3.2 XRD characterization

Fig. 3 showed the wide-angle XRD patterns of synthesized samples. The reflections at 2θ=28.5 °, 33.1 °, 47.5 °, 56.3 °, 59.1 °, 69.4 °, 76.7 ° were detected in pure CeO_2-NFs. All these peaks fitted well with CeO_2 (111), (200), (220), (311), (222), (400), (331) (JCPDS 34-0394), which indicate the typical cubic fluorite-like structure of CeO_2. When Cu/(Cu+Ce) molar ratio varied from 0 to 0.50, several diffraction peaks of CeO_2 were detected while the diffraction peaks of CuO were quite weak. This may be due to: (a) good dispersion of small sizes CuO particles on the surface of CeO_2; (b) the incorporation of Cu ion in the CeO_2 lattice in the form of Cu-Ce-O solid solution. But when Cu/(Cu+Ce) molar ratio was over 0.5, the CuO corresponding diffraction peaks at 2θ=32.5°, 38.5°(JCPDS 45-0937) become obvious, indicating copper oxides start to separate and form part of bulk CuO particles. Additionally, the lattice parameters of cerium oxide (d_{111}) of all samples were calculated and listed in Table 1. After partially incorporation of copper ions in CeO_2 lattice, d_{111} decreases

slightly since the radius of six-coordinated Cu^{2+} (0.73 Å) and Cu^{+} (0.77 Å) is smaller than that of six-coordinated Ce^{3+} (1.10 Å) or Ce^{4+} (1.01 Å). Meanwhile, the shift of diffraction peaks of CeO_2 (111) toward higher degree was observed, which is corresponded well with Bragg's law ($2d \sin\theta = n\lambda$). These evidences proved that a part of Cu ions are incorporated in CeO_2 lattice and form Cu-Ce-O solid solution[24].

Comparing with $Cu_{0.50}$-sol and $Cu_{0.50}$-cmb, the diffraction peaks of nanofibers catalysts are weaker and broader, which implies copper and cerium oxide particles of nanofibers are smaller and better dispersed. In addition, the CeO_2 lattice parameter of $Cu_{0.50}$-NFs (5.407 Å), which is smaller than that of $Cu_{0.50}$-sol (5.4201 Å) and $Cu_{0.50}$-cmb (5.413 Å), indicates the amount of Cu-Ce-O solid solution in $Cu_{0.50}$-NFs is more than that in $Cu_{0.50}$-sol and $Cu_{0.50}$-cmb catalysts.

The better dispersion of copper oxide and formation of Cu-Ce-O solid solution can strengthen the interactions between CuO and CeO_2 intensively. Which make Ce-O and Cu-O bonds become weaker and easier to crack to produce active oxygen species[25]. These active oxygen species can improve the reducibility and catalytic activity of $CuCeO_x$ catalysts.

3.3 N_2 sorption and EDX characterization

The adsorption-desorption isotherms of nanofibers catalysts were illustrated in Fig. 4. All nanofibers catalysts showed typical type IV isotherms. Their hysteresis could be identified as H3 type on the basis of IUPAC classification, which indicates the possible formation of open slit-shaped pores. The average pore diameter (d_{pore}) and specific surface areas (S_{BET}) of nanofibers catalysts were shown in Table 1 based on the calculation from the isotherms. The average pore diameter of nanofibers catalysts varies from 8.1 to 26.1 nm with different copper content. The specific surface area of nanofibers catalysts is around 24.9-74.5 m^2/g. It increases gradually from 38.9 to 74.5 m^2/g with increase of Cu/(Cu+Ce) molar ratio from 0 to 0.50 as the decreasing average diameter of nanofibers. However, when the Cu/(Cu+Ce) molar ratio further increased from 0.50 to 0.85, S_{BET} decreases drastically. This may be due to the destruction of nanofibrous morphology caused by introducing of excess copper ions. Additionally, the specific surface area of nanofibers is much higher than that of $Cu_{0.50}$-sol (20.2 m^2/g) and $Cu_{0.50}$-cmb (2.4 m^2/g). Therefore, it can be deduced that the electrospinning method endows the Cu-Ce composite catalyst with specific

nanofibrous morphology and enough surface area, which in turn promote the activity of reactions.

The bulk composition of the $CuCeO_x$ catalysts was determined by EDX analysis. Table 1 summarized the Cu atomic relative ratio (Cu_{EDX}) determined by EDX. The results showed that the nominal compositions of all catalysts agree well with the relative molar ratio determined by EDX except for $Cu_{0.15}$-NFs and $Cu_{0.30}$-NFs.

3.4 XPS characterization

The information of surface composition and chemical state of the $CuCeO_x$ catalysts were studied by XPS. The measured elements in the samples are oxygen (O 1s), cerium (Ce 3d), copper (Cu 2p) , and carbon (C 1s) in the binding energy from 0 to 1000 eV (other than CeO_2-NFs). Oxygen, cerium, copper were expected from the chemical composition of the synthesized $CuCeO_x$ catalysts. The C 1s peak was used for calibration.

The O 1s spectras of various samples, which can be resolved into two peaks by deconvolution, were shown in Fig. 5.A. The peaks at 529.4 eV can be attributed to lattice oxygen (denoted as O_{latt}), and the shoulder peaks at 531.2-532.1 eV can be assigned to the active surface adsorbed oxygen (denoted as O_{ads})[26]. The active O_{ads} contents ($O_{ads}/(O_{latt}+O_{ads})$) at the surface of synthesized catalysts were listed in Table 1. With the increase of Cu/(Cu+Ce) molar ratio from 0 to 0.50, the active O_{ads} percentage of nanofibers increases from 35.34% to 52.43%, then it decreases with further increase of the copper content. Among all the nanofibers，$Cu_{0.50}$-NFs possesses the largest amount of O_{ads} (52.43%), which is more than that of $Cu_{0.50}$-sol and $Cu_{0.50}$-cmb.

According to literature[27], the complex spectrum of Ce 3d could be decomposed into ten peaks. The two sets of spin–orbital multiplets, corresponding to the $3d_{3/2}$ and $3d_{5/2}$ contributions are labeled as u and v, respectively. The u_2, u_0, v_2, v_0 peaks can be ascribed to Ce^{3+} and u_1, u_3, u_4, v_1, v_3, v_4 peaks can be attributed to Ce^{4+}. The Ce^{3+} relative content was then estimated by $Ce^{3+}/(Ce^{3+}+Ce^{4+})\times100\%$, where $Ce^{3+}=(u_2+u_0+v_2+v_0)$ and $Ce^{4+}=(u_1+u_3+u_4+v_1+v_3+v_4)$. Ce^{3+} contents of $CuCeO_x$ catalysts at the surface were listed in Table 1, the results illustrated that $Cu_{0.30}$-NFs and $Cu_{0.50}$-NFs possess the largest amount of Ce^{3+} (18.38%) among all the nanofibers，which is much higher than that of $Cu_{0.50}$-sol (7.96%) and $Cu_{0.50}$-cmb (4.40%). The existence of

Ce^{3+}in CeO_2 implies the formation of oxygen vacancies[28]. These oxygen vacancies, which are directly related to the catalytic activity at low temperatures[29], may induce more surface adsorbed oxygen species[30].

The Cu 2p binding energy of various catalysts was shown in Fig. 5.C. The principal peaks at 934.0 eV, 934.6 eV can be identified as Cu^{2+} $2p^{3/2}$, the peaks at 953.7 eV stand for Cu^{2+} $2p^{1/2}$ and the shake-up peaks from 940.0 eV to 945.0 eV indicate the presence of reduced copper species.

The relative atomic ratios of Cu at the surface were summarized in Table 1. The results showed Cu_{XPS} ratios of nanofibers catalysts are lower than their corresponding nominal ratios and Cu_{EDX} ratios, suggesting that Cu-Ce-O solid solution could be formed on the surface of nanofibers catalysts. which is also discovered by other researchers[24]. However, the Cu_{XPS} ratios of catalysts prepared by sol-gel and urea-nitrate combustion method are much higher than their corresponding nominal ratio and Cu_{EDX} ratios, indicating the enrichment of Cu spices or formation of large bulk of copper oxide on the surface of these catalysts.

Comparing with the XPS results of O 1s and Ce 3d, it can be concluded that the active O_{ads} contents enhances with the increase of Ce^{3+} relative content, and the augmentation of these two species can be explained by charge compensation theory. In the case of $CuCeO_x$ catalysts, active copper species can incorporate in cerium oxide lattice and destruct the lattice structure, thus influence the electroneutrality. In order to retain electroneutrality, charge compensation achieved by either formation of oxygen vacancies or shift of cerium to lower oxidation state is required. In consequence, the active oxygen adsorbed on surface oxygen vacancies and cerium ions with unusual oxidation state (Ce^{3+}) can increase simultaneously.

3.5 TPR characterization

In order to check the reduction properties of the prepared catalysts, all samples were investigated by H_2-TPR. The H_2-TPR profiles were displayed in Fig. 6. H_2-TPR patterns illustrated pure cerium oxide nanofibers catalyst possesses three TPR peaks above 300 ℃. The peaks at 400 and 501 ℃ are attributed to the reduction of surface oxygen species, and the peak at 743 ℃ is ascribed to the reduction of bulk oxygen species[31]. After the addition of copper, the reduction peaks ascribed to cerium oxide can be also seen in the H_2-TPR profiles. However, two or three new reduction peaks

emerged in the nanofibers catalysts below 300 ℃. The hydrogen consumption peaks (with shoulder peaks) at the range of 190-285 ℃ can be attributed to the reduction of bulk CuO. While the reduction peaks of all $CuCeO_x$ nanofibers catalysts during the range of 145-183 ℃ indicate the highly dispersed active of Cu species[32]. Interestingly, with the increase of copper content, the main peaks shift to higher temperatures and the minor peaks which at lower temperatures than main peaks disappear gradually. This manner is fitted well with what has been found in $CuCeO_x$ catalysts prepared by combustion method[14].

The reduction features of $Cu_{0.50}$-sol and $Cu_{0.50}$-cmb are different from nanofibers, they have only one reduction peak below 300 ℃, at 235 ℃ and 276 ℃ respectively, suggesting large amount of bulk CuO was formed in these two catalysts. In addition, the main reduction peaks of $Cu_{0.50}$-sol and $Cu_{0.50}$-cmb appear at higher temperatures than the major peak (at 203 ℃) of $Cu_{0.50}$-NFs, indicating the reducibility of nanofibers catalysts is much stronger than catalyst synthesized via sol-gel and urea-nitrate combustion method.

3.6 Catalytic performance

The catalytic activities of prepared catalysts were tested in the temperature range from 100 to 280 ℃, the acetone conversion pattern was shown in Fig. 7, and the T_{50} and T_{90} (temperatures at 50% and 90% conversion of acetone) of catalyst calculated from the conversion curves were listed in table 1. In the tested temperature range, CeO_2-NFs possess the lowest catalytic activity among all the nanofibers (T_{90}=270 ℃), and with the increase of Cu/(Cu+Ce) molar ratio from 0 to 0.50, their acetone conversion curves shift progressively toward lower temperatures. Further increasing copper content diminishes the catalytic activity of nanofibers. $Cu_{0.50}$-NFs possesses the best acetone oxidation activity (T_{90}=225 ℃), and 100% acetone conversion is achieved at around 270 ℃. The acetone conversion activity sequence over the nanofibers catalysts is $Cu_{0.50}$-NFs > $Cu_{0.30}$-NFs > $Cu_{0.15}$-NFs > $Cu_{0.70}$-NFs > $Cu_{0.85}$-NFs > CeO_2-NFs. In addition, T_{50} acetone conversion of $Cu_{0.50}$-sol and $Cu_{0.50}$-cmb are 220 ℃ and 240 ℃ respectively, which are much lower than that of $Cu_{0.50}$-NFs (T_{50}=190 ℃). Since the GHSV, concentration of acetone and oxygen are different, it is hard to compare the acetone oxidation activity between $Cu_{0.50}$-NFs and catalysts in other literatures precisely. However, $Cu_{0.50}$-NFs does have excellent performance toward acetone oxidation, which can be comparable to $Cu_{0.13}Ce_{0.87}O_y$[37]

and Ce-MSP[38].

According to the characteristic and catalytic performance results, the high activity of nanofibers catalysts can be attributed to synergistic effect of (a) specific nanofibrous morphology; (b) abundant oxygen vacancies and cations with unusual oxidation states, which are both caused by the finely dispersed Cu species and formation of Cu-Ce-O solid solution. The reasons are addressed as follows.

Morphology characterization illustrated the $CuCeO_x$ nanofibers catalysts possess one-dimensional nanofibrous morphology with large specific surface area. As is well-known, nanofibrous morphology favors the catalytic reaction because it can provide large specific surface area[33] and prevent the inhibition of the mass-transfer process[34], i.e. diffusion and adsorption/desorption of reactants/products. On one side, the large specific surface area is conductive to the dispersion of active phase and hence provides more active sites for reaction. On the other side, the open structure composed by bonding the intersecting nanofibers facilitates the diffusion of gas molecules. In addition, the special nanofibrous morphology not only makes the adsorption of reactant toward the exterior or interior surfaces of nanofibers bundles easier, but also benefits the separation of product. Consequently, the mass-transfer process will be enhanced and the reactions can be accelerated. In conclusion, the nanofibrous morphology with large specific surface area is one of the pivotal factors governing the catalytic activity, and the electrospinning is an appropriate method to obtain nanofibrous morphology which can provide large specific area.

It is widely known that during VOCs catalytic oxidation reactions over metal oxides, VOCs are firstly oxidized by the lattice oxygen of metal oxides, and then the latter is re-oxidized by the gas-phase oxygen[35, 36]. In this oxygen transfer cycle, two factors play the governing roles. One is oxygen vacancies as they can accelerate the dissociation of oxygen molecules on the surface and increase the mobility of lattice oxygen. The other is the unusual oxidation states of transmission metal ions as facile redox cycle can be formed between the cations with different valences. The results of XRD indicated the existence of highly dispersed Cu species and incorporated Cu species of Cu-Ce-O solid solution in nanofibers catalysts. These Cu spices can lead to the substitution of Ce^{4+} with Cu^{2+} and structural defects of CeO_2 lattice, thus influence the electron balance of the lattice. In order to retain electroneutrality, there are two strategies: (a) the oxygen vacancies will increase and then some oxygen spices will be adsorbed on surface oxygen vacancies. So, the percentage of surface adsorbed oxygen

in $Cu_{0.50}$-NFs is more than that of $Cu_{0.50}$-sol and $Cu_{0.50}$-cmb. (b) The amount of unusual oxidation states cations will be enhanced. Therefore, the Ce^{3+} relative content of $Cu_{0.50}$-NFs is more than that of $Cu_{0.50}$-sol and $Cu_{0.50}$-cmb. As mentioned above, the enhancement of oxygen vacancies and unusual oxidation states cations will improve the activity of oxidation reaction, thus T_{50} of $Cu_{0.50}$-NFs is lower than that of $Cu_{0.50}$-sol and $Cu_{0.50}$-cmb.

4 Conclusions

$CuCeO_x$ nanofibers catalysts were successfully synthesized via electrospinning of alcohol/water solutions of Cu salt, Ce salt, and PVP. The catalytic activity test proved $Cu_{0.50}Ce_{0.50}O_x$ nanofibers catalyst (NFs) has the highest activity (T_{50}=190 ℃) for acetone abatement among all these nanofibers catalysts. Besides, this catalyst is much more active than $Cu_{0.50}Ce_{0.50}O_x$ synthesized via sol-gel (T_{50}=220 ℃) and urea-nitrate combustion method (T_{50}=240 ℃). The reason can be concluded as: (1) nanofibrous morphology with large specific surface area, (2) abundant oxygen vacancies and (3) cations with unusual oxidation states. $Cu_{0.50}$-NFs possesses the largest specific surface area (74.5 m^2/g) among all nanofibers catalysts. Its specific surface area is about 3.7 and 31.3 times of those of the catalysts synthesized via sol-gel (sol) and combustion (cmb) methods. XRD patterns showed Cu species disperse uniformly over all nanofibers catalysts, and the degree of metal oxide aggregation is weaker than that of $Cu_{0.50}$-sol and $Cu_{0.5}$-cmb. The decreased lattice parameter of cerium oxide suggests large portion of Cu over nanofibers catalysts are incorporated into CeO_2 lattice in the form of Cu-Ce-O solid solution, leading to structure defects and interface oxygen vacancies. The amount of surface adsorbed oxygen (O_{ads}) and Ce^{3+} relative content in nanofibers catalysts vary with the increase of Cu/(Cu+Ce) molar ratio. According to XPS results, $Cu_{0.50}$-NFs catalyst possesses the highest O_{ads} percentage (52.4%) and Ce^{3+} relative content (18.38%), which indicates the high density of oxygen vacancies and abundant cations with unusual oxidation states. Thus electrospinning is an effective method to prepare nanofibers $CuCeO_x$ catalysts with good acetone oxidation activity. This method can be extended to other metal oxide or noble metal catalysts for various catalytic reactions.

Acknowledgement

This work was supported by National Science Fund for Distinguished Young Scholars (no. 51125025) and the Key Innovation Team for Science and Technology of Zhejiang Province (Grant No. 2011R50017).

Figure captions

Fig. 1. SEM images of as-spun nanofibers: (a) CeO_2, (b)$Cu_{0.15}$, (c) $Cu_{0.30}$, (d) $Cu_{0.50}$, (e) $Cu_{0.70}$, (f) $Cu_{0.15}$; calcinated nanofibers: (A) CeO_2, (B)$Cu_{0.15}$, (C) $Cu_{0.30}$, (D) $Cu_{0.50}$, (E) $Cu_{0.70}$, (F) $Cu_{0.15}$;

Fig. 2. TEM images of single $Cu_{0.50}$-NFs

Fig. 3. XRD patterns of (a) CeO_2-NFs, (b) $Cu_{0.15}$-NFs, (c) $Cu_{0.30}$-NFs, (d) $Cu_{0.50}$-NFs, (e) $Cu_{0.70}$-NFs, (f) $Cu_{0.85}$-NFs, (g) $Cu_{0.50}$-sol, (h) $Cu_{0.50}$-cmb

Fig. 4. N_2 adsorption-desorption isotherms of (a) CeO_2-NFs, (b) $Cu_{0.15}$-NFs, (c) $Cu_{0.30}$-NFs, (d) $Cu_{0.50}$-NFs, (e) $Cu_{0.70}$-NFs, (f) $Cu_{0.85}$-NFs

Fig. 5. (A) O 1s, (B) Ce 3d, (C) Cu 2p XPS spectra of (a) CeO_2-NFs, (b) $Cu_{0.15}$-NFs, (c) $Cu_{0.30}$-NFs, (d) $Cu_{0.50}$-NFs, (e) $Cu_{0.70}$-NFs, (f) $Cu_{0.85}$-NFs, (g) $Cu_{0.50}$-sol, (h) $Cu_{0.50}$-cmb

Fig. 6. H_2-TPR patterns of (a) CeO_2-NFs, (b) $Cu_{0.15}$-NFs, (c) $Cu_{0.30}$-NFs, (d) $Cu_{0.50}$-NFs, (e) $Cu_{0.70}$-NFs, (f) $Cu_{0.85}$-NFs, (g) $Cu_{0.50}$-sol, (h) $Cu_{0.50}$-cmb

Fig. 7. Conversion of acetone as a function of reaction temperature (500ppm acetone, 5%O_2, N_2 balance, GHSV=79,000 ml/(g ħ))

References

1. G. Zhou, H. Lan, X. Yang, Q. Du, H. Xie and M. Fu, *Ceramics International*, 2013, **39**, 3677-3683.
2. H. Huang, F. Haghighat and P. Blondeau, *Indoor Air*, 2006, **16**, 236-247.
3. Y.-S. Chen and H.-S. Liu, *Industrial & engineering chemistry research*, 2002, **41**, 1583-1588.
4. T. Oda, *Journal of Electrostatics*, 2003, **57**, 293-311.
5. C. Zheng, X. Zhu, X. Gao, L. Liu, Q. Chang, Z. Luo and K. Cen, *Journal of Industrial and Engineering Chemistry*, 2013.
6. C. He, F. Zhang, L. Yue, X. Shang, J. Chen and Z. Hao, *Applied Catalysis B: Environmental*, 2012, **111–112**, 46-57.
7. G. C. Pontelli, R. P. Reolon, A. K. Alves, F. A. Berutti and C. P. Bergmann, *Applied Catalysis A: General*, 2011, **405**, 79-83.
8. B. Solsona, M. Perez-Cabero, I. Vazquez, A. Dejoz, T. Garcia, J. Alvarez-Rodriguez, J. El-Haskouri, D. Beltran and P. Amoros, *Chemical Engineering Journal*, 2012, **187**, 391-400.
9. S. Xu, D. Sun, H. Liu, X. Wang and X. Yan, *Catalysis Communications*, 2011, **12**, 514-518.
10. J. Sun, L. Bo, L. Yang, X. Liang and X. Hu, *Rsc Advances*, 2014, **4**, 14385-14391.

11. A. A. Taha, A. A. Hriez, H. Wang, Y.-n. Wu and F. Li, *Rsc Advances*, 2014, **4**, 5901-5905.
12. P. M. Heynderickx, J. W. Thybaut, H. Poelman, D. Poelman and G. B. Marin, *Journal of catalysis*, 2010, **272**, 109-120.
13. D. Delimaris and T. Ioannides, *Applied Catalysis B: Environmental*, 2008, **84**, 303-312.
14. D. Delimaris and T. Ioannides, *Applied Catalysis B: Environmental*, 2009, **89**, 295-302.
15. M. Raciulete and P. Afanasiev, *Applied Catalysis A: General*, 2009, **368**, 79-86.
16. S. M. Saqer, D. I. Kondarides and X. E. Verykios, *Applied Catalysis B: Environmental*, 2011, **103**, 275-286.
17. X. Zhang, V. Thavasi, S. G. Mhaisalkar and S. Ramakrishna, *Nanoscale*, 2012, **4**, 1707-1716.
18. Y. Wang, Y. R. Su, L. Qiao, L. X. Liu, Q. Su, C. Q. Zhu and X. Q. Liu, *Nanotechnology*, 2011, **22**, 225702.
19. C. He, J. Li, P. Li, J. Cheng, Z. Hao and Z.-P. Xu, *Applied Catalysis B: Environmental*, 2010, **96**, 466-475.
20. H. Li, G. Lu, Q. Dai, Y. Wang, Y. Guo and Y. Guo, *Applied Catalysis B: Environmental*, 2011, **102**, 475-483.
21. Y. Dai, W. Liu, E. Formo, Y. Sun and Y. Xia, *Polymers for Advanced Technologies*, 2011, **22**, 326-338.
22. X. Wu, Q. Liang, D. Weng and Z. Lu, *Catalysis Communications*, 2007, **8**, 2110-2114.
23. A. Yousef, N. A. M. Barakat, T. Amna, S. S. Al-Deyab, M. S. Hassan, A. Abdel-hay and H. Y. Kim, *Ceramics International*, 2012, **38**, 4525-4532.
24. C. He, Y. Yu, L. Yue, N. Qiao, J. Li, Q. Shen, W. Yu, J. Chen and Z. Hao, *Applied Catalysis B: Environmental*, 2014, **147**, 156-166.
25. Z. Wang, G. Shen, J. Li, H. Liu, Q. Wang and Y. Chen, *Applied Catalysis B: Environmental*, 2013, **138–139**, 253-259.
26. W. Xingyi, K. Qian and L. Dao, *Applied Catalysis B: Environmental*, 2009, **86**, 166-175.
27. L. Qi, Q. Yu, Y. Dai, C. Tang, L. Liu, H. Zhang, F. Gao, L. Dong and Y. Chen, *Applied Catalysis B: Environmental*, 2012, **119**, 308-320.
28. L.-H. Chang, N. Sasirekha, Y.-W. Chen and W.-J. Wang, *Industrial & engineering chemistry research*, 2006, **45**, 4927-4935.
29. R. Qu, X. Gao, K. Cen and J. Li, *Applied Catalysis B: Environmental*, 2013, **142**, 290-297.
30. H. He, H. Dai and C. Au, *Applied Catalysis B: Environmental*, 2001, **33**, 65-80.
31. A. Trovarelli and P. Fornasiero, *Catalysis by ceria and related materials*, World Scientific, 2013.
32. Z.-Q. Zou, M. Meng and Y.-Q. Zha, *The Journal of Physical Chemistry C*, 2009, **114**, 468-477.
33. H. Xiang, Y. Long, X. Yu, X. Zhang, N. Zhao and J. Xu, *CrystEngComm*, 2011, **13**, 4856-4860.
34. C. Pham-Huu, N. Keller, G. Ehret, L. c. J. Charbonniere, R. Ziessel and M. J. Ledoux, *Journal of Molecular Catalysis A: Chemical*, 2001, **170**, 155-163.
35. V. Santos, M. Pereira, J. Órfão and J. Figueiredo, *Applied Catalysis B: Environmental*, 2010, **99**, 353-363.
36. S. C. Kim and W. G. Shim, *Applied Catalysis B: Environmental*, 2010, **98**, 180-185.
37. C. Hu, Q. Zhu, Z. Jiang, L. Chen and R. Wu, *Chemical Engineering Journal*, 2009, **152**, 583-590.
38. C. Wang and H. Bai, *Industrial & Engineering Chemistry Research*, 2011, **50**, 3842-3848.

Figure

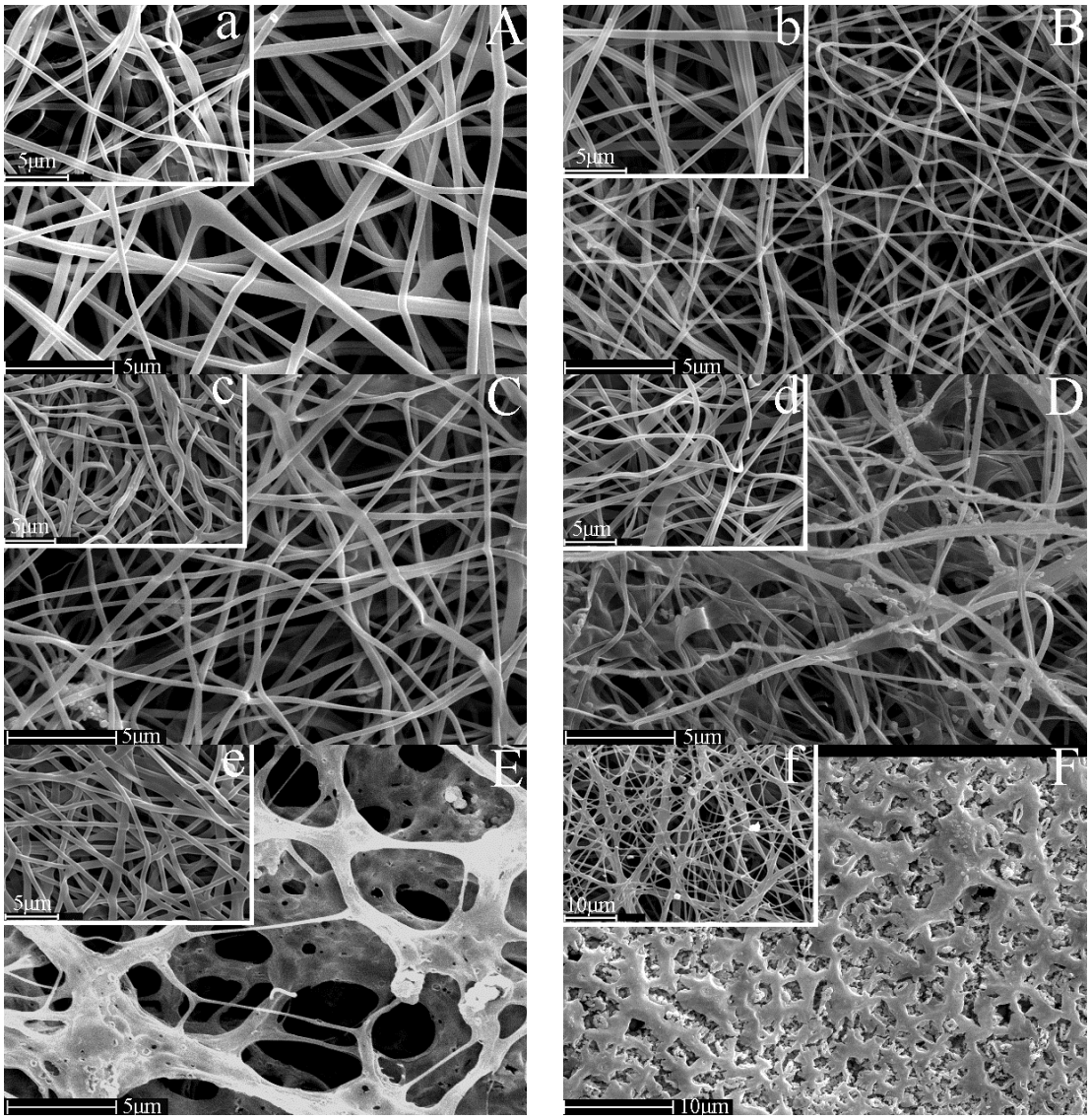

Fig 1. SEM images of as-spun nanofibers: (a) CeO_2, (b)$Cu_{0.15}$, (c) $Cu_{0.30}$, (d) $Cu_{0.50}$, (e) $Cu_{0.70}$, (f) $Cu_{0.15}$; calcinated nanofibers: (A) CeO_2, (B)$Cu_{0.15}$, (C) $Cu_{0.30}$, (D) $Cu_{0.50}$, (E) $Cu_{0.70}$, (F) $Cu_{0.15}$;

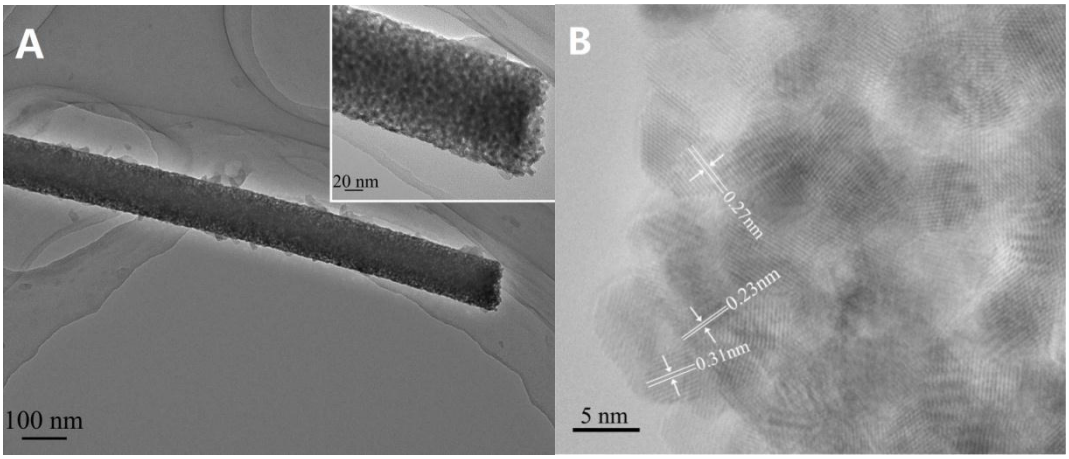

Fig. 2. TEM images of single $Cu_{0.50}$-NFs

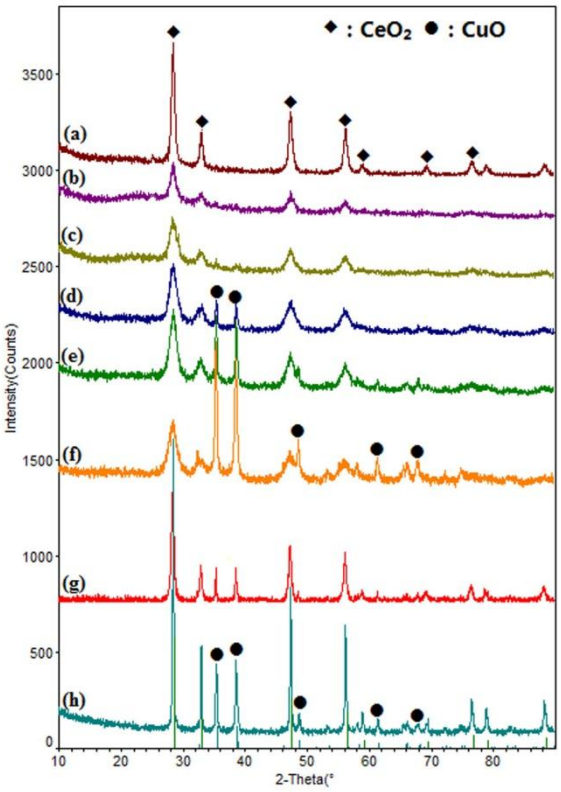

Fig. 3. XRD patterns of (a) CeO_2-NFs, (b) $Cu_{0.15}$-NFs, (c) $Cu_{0.30}$-NFs, (d) $Cu_{0.50}$-NFs, (e) $Cu_{0.70}$-NFs, (f) $Cu_{0.85}$-NFs, (g) $Cu_{0.50}$-sol, (h) $Cu_{0.50}$-cmb

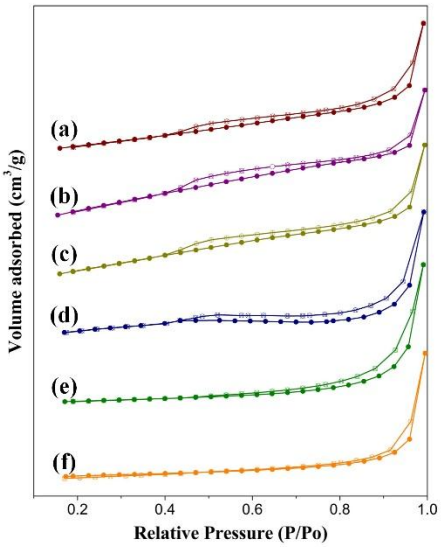

Fig. 4. N_2 adsorption-desorption isotherms of (a) CeO_2-NFs, (b) $Cu_{0.15}$-NFs, (c) $Cu_{0.30}$-NFs, (d) $Cu_{0.50}$-NFs, (e) $Cu_{0.70}$-NFs, (f) $Cu_{0.85}$-NFs

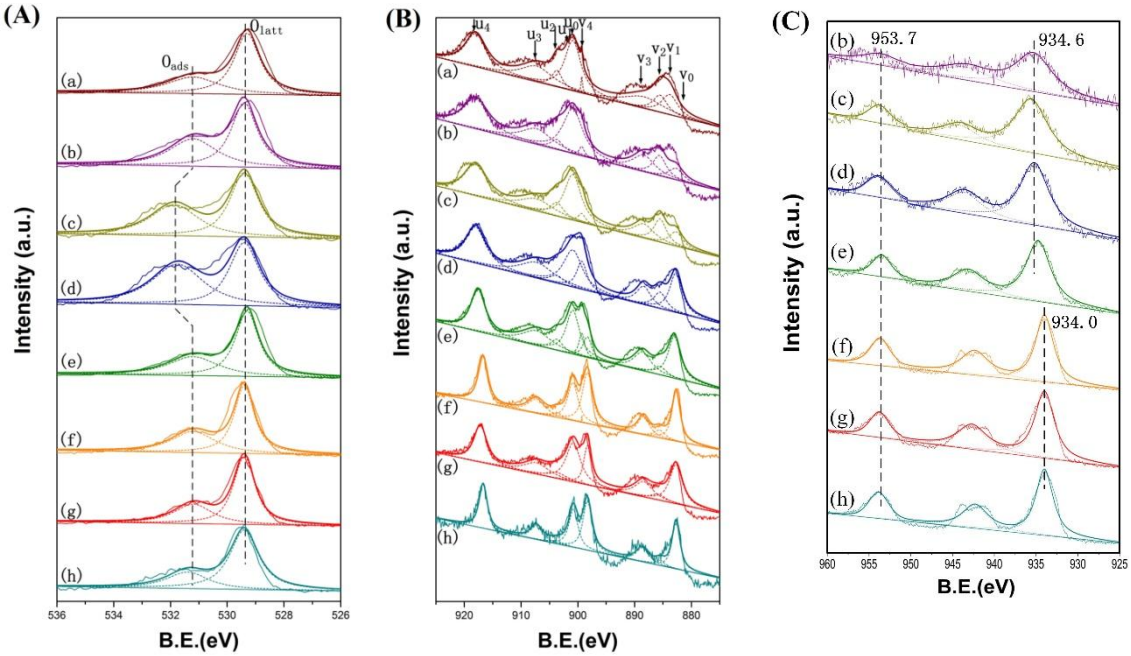

Fig. 5. (A) O 1s, (B) Ce 3d, (C) Cu 2p XPS spectra of (a) CeO_2-NFs, (b) $Cu_{0.15}$-NFs, (c) $Cu_{0.30}$-NFs, (d) $Cu_{0.50}$-NFs, (e) $Cu_{0.70}$-NFs, (f) $Cu_{0.85}$-NFs, (g) $Cu_{0.50}$-sol, (h) $Cu_{0.50}$-cmb

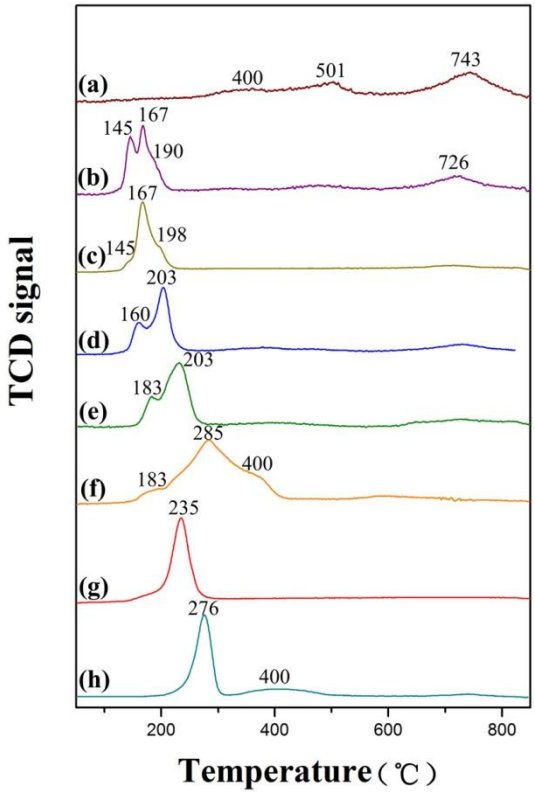

Fig. 6. H_2-TPR patterns of (a) CeO_2-NFs, (b) $Cu_{0.15}$-NFs, (c) $Cu_{0.30}$-NFs, (d) $Cu_{0.50}$-NFs, (e) $Cu_{0.70}$-NFs, (f) $Cu_{0.85}$-NFs, (g) $Cu_{0.50}$-sol, (h) $Cu_{0.50}$-cmb

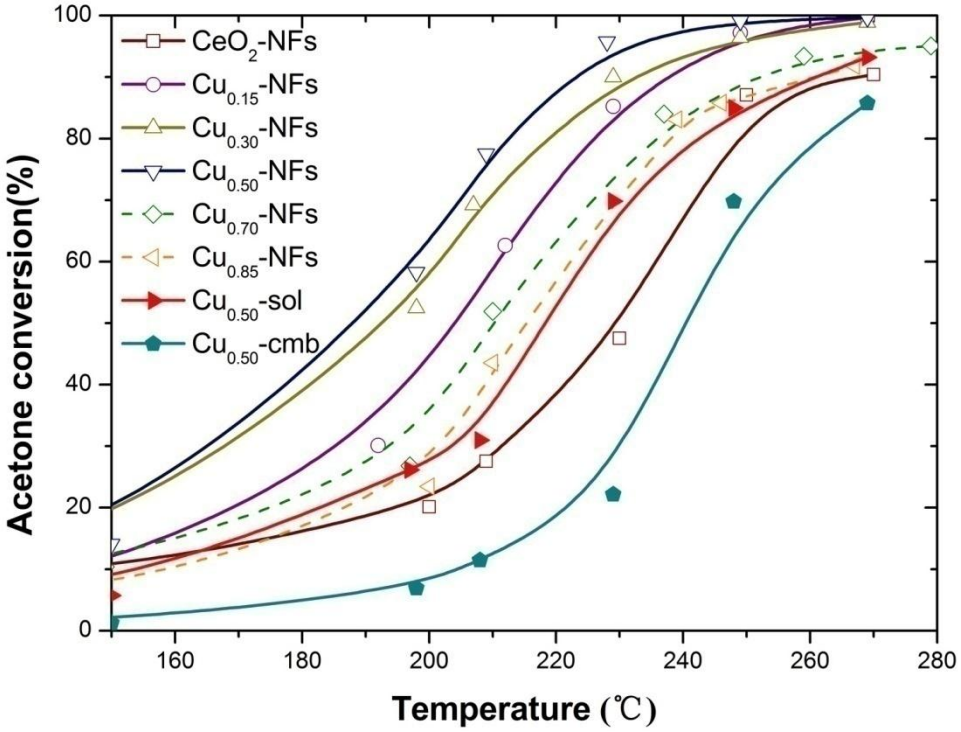

Fig. 7. Conversion of acetone as a function of reaction temperature (500ppm acetone, 5%O_2, N_2 balance, GHSV=79,000 ml/(g ħ))

Table

Table 1. Summary of the N_2 sorption, SEM, XRD, XPS, and catalytic performance results

Sample	S_{BET} (m^2/g)	$D_{as\text{-}spun}$ [a] (nm)	$D_{calcinated}$ [b] (nm)	d_{pore} [c] (nm)	d_{111} [d] (Å)	Cu_{EDX} (at%)	Cu_{XPS} (at%)	O_{ads} [e] (%)	Ce^{3+} [f] (%)	T_{50} (℃)	T_{90} (℃)
CeO_2-NFs	38.9	610	460	9.1	5.424	-	-	35.43	-	230	270
$Cu_{0.15}$-NFs	46.3	590	345	8.9	5.420	19.77	14.42	42.81	14.10	205	240
$Cu_{0.30}$- NFs	52.5	545	340	8.1	5.411	34.32	27.31	44.70	18.38	195	230
$Cu_{0.50}$- NFs	74.5	530	295	8.4	5.407	47.99	33.07	52.43	18.38	190	225
$Cu_{0.70}$- NFs	37.5	525	-	10.7	5.409	70.17	51.28	37.78	12.19	210	250
$Cu_{0.85}$- NFs	24.9	-	-	26.1	5.422	84.27	77.17	39.75	5.61	215	260
$Cu_{0.50}$ –sol	20.2	-	-	-	5.420	49.62	77.67	33.70	8.00	220	260
$Cu_{0.50}$-cmb	2.4	-	-	-	5.413	50.33	87.10	27.77	4.40	240	-

[a] Average diameter of as-spun nanofibers

[b] Average diameter of calcinated nanofibers

[c] Average pore diameter of nanofibers

[d] The lattice parameters of CeO_2 (111)

[e] The percentage of adsorbed oxygen measured by XPS

[f] The percentage of Ce^{3+} measured by XPS

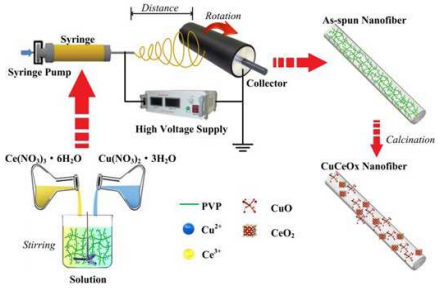

Highlights

A series of $CuCeO_x$ nanofibers catalysts with excellent performance toward acetone oxidation were prepared by electrospinning method.